

PbCu₃TeO₇: An $S = \frac{1}{2}$ staircase Kagome lattice with significant intra- and inter-plane couplings

B. Koteswararao,¹ R. Kumar,² Jayita Chakraborty,³ Byung-Gu Jeon,⁴
A. V. Mahajan,² I. Dasgupta,³ Kee Hoon Kim,⁴ and F. C. Chou^{1,5,*}

¹*Center of Condensed Matter Sciences,*

National Taiwan University, Taipei 10617, Taiwan

²*Department of Physics, Indian Institute of Technology Bombay, Mumbai 400076, India*

³*Department of Solid State Physics, Indian Association for
the Cultivation of Science, Jadavpur, Kolkata 700 032, India*

⁴*CeNSCMR, Department of Physics and Astronomy,
Seoul National University, Seoul 151-747, Republic of Korea*

⁵*National Synchrotron Radiation Research Center, Hsinchu 30076, Taiwan*

(Date textdate; Received textdate; Revised textdate; Accepted textdate; Published textdate)

Abstract

We have synthesized polycrystalline and single crystal samples of PbCu₃TeO₇ and studied its properties via magnetic susceptibility $\chi(T)$ and heat-capacity $C_p(T)$ measurements and also electronic structure calculations. Whereas the crystal structure is suggestive of the presence of a quasi-2D network of Cu²⁺ ($S = 1/2$) buckled staircase Kagome layers, the $\chi(T)$ data show magnetic anisotropy and three magnetic anomalies at temperatures, $T_{N1} \sim 36$ K, $T_{N2} \sim 25$ K, $T_{N3} \sim 17$ K, respectively. The $\chi(T)$ data follow the Curie-Weiss law above 200 K and a Curie-Weiss temperature $\theta_{CW} \sim -150$ K is obtained. The data deviate from the simple Curie-Weiss law below 200 K, which is well above T_{N1} , suggesting the presence of competing magnetic interactions. The magnetic anomaly at T_{N3} appears to be of first-order from magnetization measurements, although our heat-capacity $C_p(T)$ results do not display any anomaly at T_{N3} . The hopping integrals obtained from our electronic structure calculations suggest the presence of significant intra-Kagome (next-nearest neighbor and diagonal) and inter-Kagome couplings. These couplings take the PbCu₃TeO₇ system away from a disordered ground state and lead to long-range order, in contrast to what might be expected for an ideal (isotropic) 2D Kagome system.

PACS numbers: 71.27.+a 75.10.Jm 75.50.Ee

Keywords: PbCu₃TeO₇, frustration, Kagome, quantum spin

I. INTRODUCTION

Frustrated magnetism in Kagome Heisenberg antiferromagnetic systems (KHAF) has been a major subject in condensed matter physics due to their unconventional, exotic ground states which emerge from the interplay between geometrical frustration and low-dimensional quantum effects.^{1,2} In particular, quantum fluctuations for $S = 1/2$ systems are found to be strong among KHAF and can lead to interesting behavior like that of a spin liquid.³ Theoretical studies on ideal $S = 1/2$ isotropic KHAF lattice have demonstrated that it has a Resonating Valence Bond (RVB)-like disordered ground state.^{4,5} Recent numerical studies⁶ have also predicted that its ground state is a spin liquid with a small spin-gap (Δ/k_B) of $(0.03 \sim 0.05)J/k_B$ to its triplet excited state (where J is the exchange interaction between nearest-neighbor (nn) spins). A limited number of experimental realizations of structurally ideal, $S = 1/2$, KHAF have been found, which include Zn and Mg-Herberthsmithite, Kapellasite, and Haydeeite.⁷⁻⁹ Among these, Zn-Herberthsmithite $\text{ZnCu}_3(\text{OH})_6\text{Cl}_2$ is the best example to explain isotropic $S = 1/2$ KHAF behavior. Experimental studies on Zn-Herberthsmithite have shown that there is no magnetic ordering down to $\frac{J/k_B}{3000}$ K, which implies that it has a disordered ground state.¹⁰ But an unambiguous proof for the existence of a spin-gap from an experimental point of view is lacking. The natural ion exchange of Cu and Zn or Mg is inevitable in these systems, which is probably the main obstacle to detect the intrinsic nature of these $S = 1/2$ KHAF. On the other hand, there are a few anisotropic KHAF systems such as Volborthite $\text{Cu}_3\text{V}_2\text{O}_7(\text{OH})_2 \cdot 2\text{H}_2\text{O}$ ¹¹ and Vesignieite $\text{BaCu}_3\text{V}_2\text{O}_8(\text{OH})_2$ ¹², which do not have much atomic site-disorder, in which the Kagome layers are built by two nearest neighbor (nn) exchange couplings. These have also been studied to understand the real ground state physics of a Kagome system. Despite the presence of significant anisotropy, these systems show interesting spin dynamics.¹³ There is another kind of anisotropic Kagome lattice in $\text{Rb}_2\text{Cu}_3\text{SnF}_{12}$,¹⁴ where the Kagome layer is formed by four exchange couplings and has a spin-gap of 20 K. The pinwheel valence bond solid (VBS) excitations are realized in this anisotropic KHAF system.¹⁵ Theoretical predictions also suggest that when the Kagome layer is perturbed with additional exchange couplings such as next-nearest neighbor nnn and diagonal couplings, the system is driven to a novel ordered state from the disordered state of isotropic Kagome layer.¹⁶ These predictions prompted us to look for newer $S = 1/2$, KHAF systems to explore interesting physics associated with the presence of anisotropy and additional couplings.

Herein, we introduce a new anisotropic magnetic system, $\text{PbCu}_3\text{TeO}_7$,¹⁸ which has $S = 1/2$ staircase (buckled) Kagome layers built by Cu and O atoms (see Fig. 1). This system has Kagome

layers similar to those of $A_3V_2O_8$ ($A=\beta\text{-Cu, Ni, Co}$).^{19,20} Detailed studies have been done on single crystals of $S = 1$ and $S = 3/2$ staircase Kagome systems $Ni_3V_2O_8$ and $Co_3V_2O_8$. The $Ni_3V_2O_8$ system has four competing magnetic transitions (two incommensurate and two commensurate) below 9 K, one of which is a multiferroic transition at $T \sim 6$ K.^{21,22} However, $Co_3V_2O_8$ does not show multiferroicity, which might be due to its high spin state with low quantum fluctuations. Less work has been done on the $S = 1/2$ analog $\beta\text{-Cu}_3V_2O_8$, probably due to non availability of single crystals.

We report here the magnetic properties of $PbCu_3TeO_7$. The magnetic susceptibility $\chi(T)$ data indicate that the dominant exchange interactions between Cu^{2+} ions are antiferromagnetic (AF) with a Curie-Weiss temperature (θ_{CW}) of about -150 K. The $\chi(T)$ deviates from Curie-Weiss behavior below ~ 200 K. We observed a total of three magnetic anomalies ($T_{N1} \sim 36$ K, $T_{N2} \sim 25$ K, and $T_{N3} \sim 16$ K) in the $\chi(T)$ data of a single crystal. The magnetic anomalies at T_{N1} and T_{N3} were evident only when the applied magnetic field H was parallel to the crystallographic a -axis, whereas the one at T_{N2} could be observed only for $H \parallel c$. The anomaly at T_{N3} is first order in nature and is field sensitive. On the other hand, heat capacity data in zero field (for both polycrystalline and single crystal samples) showed anomalies of T_{N1} and T_{N2} only. The first-order transition at T_{N3} could not be observed by us in heat capacity data. We suggest that this might be due to the small latent heat involved in this transition. Our electronic structure calculations in conjunction with our experimental findings suggest the presence of various competing magnetic couplings, in addition to nn , in $PbCu_3TeO_7$ which in turn cause a deviation from the superficially anticipated regular Kagome geometry leading to long-range order (LRO).

II. EXPERIMENTAL DETAILS

Polycrystalline samples of $PbCu_3TeO_7$ were prepared by conventional solid-state reaction method using PbO , CuO , and Te precursors. The stoichiometric amount of chemicals were ground thoroughly and fired at 750°C for 5 days with three intermediate grindings. To obtain single crystals, a mixture of $PbCu_3TeO_7$ and $NaCl/KCl$ flux in the mass ratio 1 : 2 was charged in an alumina crucible, fired at 800°C for 24 hrs and then cooled slowly to 650°C with a cooling rate of 1°C per hour. Single crystals were extracted after washing the flux with hot water. The x-ray diffraction (XRD) data were collected using *D8 Advance* (Bruker) on the single crystal and on (polycrystalline) powder obtained from crushing the crystals. Magnetic and heat-capacity measurements were performed on polycrystalline and single crystal samples using a Physical Property

Measurement System (PPMS) from Quantum Design. For heat-capacity, we employed the thermal relaxation method with two time constants (2τ model) to fit the heat-capacity data. The single crystal used for the magnetization measurements is of mass 2 mg and approximate dimensions 1.5 mm x 0.5 mm x 0.45 mm as shown in Fig. 2(b).

III. RESULTS AND DISCUSSION

A. X-ray diffraction and structural features

The single phase nature of the polycrystalline sample was confirmed by comparing the measured XRD pattern with the calculated one generated by powdercel²³ using the initial structural parameters of the orthorhombic space group $Pnma$ (space group No. 62) given by B. Wedel, *et al.*¹⁸ Rietveld refinement of the XRD pattern was done using the Fullprof suite software²⁴ (as shown in Fig. 2(a)). The lattice parameters obtained from the refinement are $a = 10.484$ Å, $b = 6.347$ Å, and $c = 8.807$ Å. The obtained atomic positions and occupancies are summarized in Table 1. These structural parameters are in good agreement with the previously published values.¹⁸ A rectangular crystal was placed on a glass slide with the top face (see Fig. 2) parallel to the plane of the slide and XRD was performed. It resulted in the appearance of only $(0ll)$ peaks as shown in Fig. 2(b)). This indicates that the top crystal surface (as indicated in Fig. 2) is perpendicular to the $[0ll]$ direction or bc -plane. This means that the a -axis lies in the as-grown plane of the crystal. Note that crystallographic a -axis is perpendicular to the staircase Kagome layers, as shown in Fig. 1(b). We have further taken the Laue pattern of the crystal, and found that the crystallographic a -axis is along the length of the crystal. The other crystallographic axes (b and c) were also identified and make roughly 45° with the top plane of the crystal, as shown in the inset of Fig. 2(b).

The staircase Kagome planes in the $\text{PbCu}_3\text{TeO}_7$ ¹⁸ structure are formed by Cu atoms (Cu1 and Cu2) as shown in Fig. 1. The Cu^{2+} ions are coupled via O^{2-} ions and form buckled layers in the bc -planes, as shown in Fig. 1(b). According to the Cu-Cu bond-lengths and the Cu-O-Cu bond-angles, the staircase Kagome plane possibly has four different nearest neighbor (nn) exchange constants J_1 , J_2 , J_3 and J_4 (see Fig. 1(b)). In this staircase Kagome plane, Cu1 atoms form linear chains with the couplings alternating between J_2 and J_4 . These Cu1 chains are connected with each other via Cu2 atoms with couplings J_1 and J_3 to form a 2D network. Other possible magnetic coupling paths are also shown in Fig. 1(f), the hopping integrals for which have been calculated by us. These are t_5 , t_6 , t_7 , and t_8 which are in addition to the nn hoppings t_1 , t_2 , t_3

and t_4 (corresponding to J_1 , J_2 , J_3 and J_4 , respectively). The Kagome planes are separated by Pb and Te atoms with a small inter-planar distance of about 4 Å, which suggests that significant three-dimensional couplings between the layers might be present.

B. Magnetic measurements:

The magnetization M was measured as a function of temperature T . The dependencies of the magnetic susceptibility $\chi(= M/H)$ in the range from 2 K to 370 K for the polycrystalline and single crystal samples of $\text{PbCu}_3\text{TeO}_7$ are shown in Fig. 3(a). Magnetic measurements were performed on the 2 mg single crystal (shown in Fig. 2(b)) for each of the crystal direction a , b , and c , respectively in an applied magnetic field H . The $\chi(T)$ data follow a Curie-Weiss behavior in high- T region. Even in the paramagnetic region, a significant anisotropy is seen between the field orientation along a and the other two perpendicular directions (b and c). This means that the intra-Kagome (bc -plane) anisotropy (difference between b - and c - axis) is small compared to the inter-Kagome anisotropy. The $\chi(T)$ data of the polycrystalline sample lie in between the single crystal data for $H \parallel a$ and $H \parallel bc$, but for $T > 200$ K they are close to the single crystal data of $H \parallel a$, while below 200 K they are closer to the single crystal data for $H \perp a$. The temperature independent magnetic susceptibility χ_0 was estimated from polycrystalline data at high- T from 300 K to 800 K (data not shown here). We subtracted $\chi_0 = -(3 \pm 0.3) \times 10^{-5} \text{ cm}^3/\text{mol Cu}$ from our measured data and then plotted $(\chi - \chi_0)^{-1}$ vs T in Fig. 3(b). The core diamagnetic susceptibility (χ_{core}) of $\text{PbCu}_3\text{TeO}_7$ is calculated to be $-5.23 \times 10^{-5} \text{ cm}^3/\text{mol Cu}$ from χ_{core} of individual ions.²⁵ The Van Vleck paramagnetic susceptibility is then estimated to be $\chi_{vv} = \chi_0 - \chi_{core} \sim (2.23 \pm 0.3) \times 10^{-5} \text{ cm}^3/\text{mol Cu}$, which is comparable with other cuprates.²⁶ The $\chi(T)$ data follow the Curie-Weiss (CW) law $\left(\frac{C}{T - \theta_{CW}}\right)$ in the T -range 200 - 370 K where C is the Curie constant and θ_{CW} is the Curie-Weiss temperature. The obtained parameters from the single crystal data are given in the Table II. The C value corresponds to an effective magnetic moment (μ_{eff}) of about $2 \mu_B/\text{Cu}$, which is slightly larger than the spin-only value for $S = 1/2$ which is $1.73 \mu_B$. The negative θ_{CW} indicates that the dominant couplings are antiferromagnetic in nature. There is a deviation from the Curie-Weiss law below 200 K, which indicates that it is not a simple paramagnet at low- T . This deviation might be a result of the competitive exchange couplings present in the quasi-2D staircase Kagome planes. The $\chi(T)$ data of polycrystalline samples exhibit a total of three magnetic anomalies at $T_{N1} \sim 36$ K, $T_{N2} \sim 25$ K, and $T_{N3} \sim 17$ K, respectively. The ordering temperature (T_{N1}) is relatively smaller than θ_{CW} and the temperature below which a deviation from CW behavior is seen (200 K), which

indicates that the system is moderately frustrated. These three magnetic anomalies (T_{N1} , T_{N2} and T_{N3}) are also seen in the single crystal data, but with significant anisotropy. All of the anomalies are not evident for each field direction. For instance, the magnetic anomaly T_{N1} is evident only when $H \parallel a$, and the anomaly at T_{N2} is seen only for $H \parallel c$. On the other hand for $H \parallel b$, no clear anomalies were observed. The anomaly at T_{N3} is prominent for $H \parallel a$ (see Fig. 4). Although, the appearance of anomalies in the $\chi(T)$ data depends on the field direction, the transitions are not field driven because the two anomalies (T_{N1} and T_{N2}) appear in zero-field heat capacity data as will be discussed in a later section. Similar H -direction dependent anomalies were also reported in a multiferroic, spiral magnet FeVO_4 .²⁷ The susceptibility χ_b ($\chi(T)$ for $H \parallel b$) increases below the transition while χ_a and χ_c decrease below the transition. This suggests that b -axis might be the hard-axis of magnetization. We have also performed dielectric constant and electric polarization versus T down to 2 K on the polycrystalline samples, neither anomaly in the dielectric constant nor electric polarization are observed below the transition temperatures.

In order to obtain insight about the transition at T_{N3} , we have measured M of a collection of carefully oriented crystals ($H \parallel a$), while cooling and warming in different H 's of 1 kOe, 5 kOe, 10 kOe, 15 kOe, respectively, as shown in Fig. 4. The transition at T_{N3} is sharp and looks different from those of at T_{N1} and T_{N2} . There is a difference in the position of the peak for the zero-field-cooled warming (ZFCW) data and the field-cooled cooling (FCC) data, while no difference is observed between ZFC warming and FC warming (FCW) data. This kind of thermal hysteresis is a characteristic feature of a first-order phase transition.²⁸ Similar sharp, first-order anomalies are also observed at 3.9 K in $\text{Ni}_3\text{V}_2\text{O}_8$ ²¹ and 6 K in $\text{Co}_3\text{V}_2\text{O}_8$ ³⁰ staircase Kagome systems. Moreover, the observed peak position moves to higher temperatures with increasing H and this variation (summarized in Table III) suggests that the observed first-order transition is ferromagnetic in nature. The T_{N3} peak also broadens and the difference between the position (in temperature) of the warming and cooling peak decreases as H increases. This kind of field-induced broadening is also a characteristic feature of the first-order transition.²⁹ Finally, the T_{N3} peak is suppressed in a field of about 20 kOe, however T_{N1} and T_{N2} peaks remain, more or less, unaffected by magnetic fields upto 70 kOe and do not exhibit any thermal hysteresis like observed for T_{N3} (data not shown here).

C. Heat-Capacity measurements

The T -dependent heat-capacity C_p of the polycrystalline $\text{PbCu}_3\text{TeO}_7$ samples in the range from 2 to 300 K is presented in Fig. 5. The $C_p(T)$ data were measured using the PPMS by the thermal relaxation method. For a magnetic insulator, one expects both lattice and magnetic contributions to the heat-capacity. We used the Debye model³¹ to obtain the lattice part in the following manner. We fit the $C_p(T)$ data in the T -range from 150 K to 300 K with a linear combination of two Debye integrals as given below

$$C_p(T) = 9rNk_B \sum_{i=1,2} C_i \left(\frac{T}{\theta_D^i} \right)^3 \int_0^{\frac{x_D^i}{T}} \frac{x^4 e^x}{(e^x - 1)^2} dx \quad (1)$$

Here r is the number of atoms per formula unit, θ_D^i is a Debye temperature, and $x_D^i = \theta_D^i/T$ ($i = 1, 2$). The fitting yields $C_1 = 0.43 \pm 0.05$, $\theta_D^1 = (280 \pm 10)$ K, $C_2 = 0.5 \pm 0.05$, and $\theta_D^2 = 772 \pm 30$ K. The fitting curve was extrapolated down to 2 K and this was then subtracted from the measured $C_p(T)$. Magnetic heat-capacity $C_m(T)$ was thus obtained (see inset of Fig. 5). Sharp anomalies are observed at 36 K and 25 K, which agree well with the anomalies found at T_{N1} and T_{N2} in $\chi(T)$. We observed the presence of $C_m(T)$ upto 150 K which is well above T_{N1} , which signifies the presence of magnetic correlations above T_{N1} and this behavior is also consistent with the magnetic data. However, we could not detect any transition at T_{N3} in the data. In fact, detailed $C_p(T)$ measurements were done around 16 K with a large number of points. The raw data of the sample temperature as a function of time at each of these temperatures showed a good fit to the 2τ model. In the case of a first-order transition, it has been documented that deviations from the simple 2τ behavior occur for C_p data at the transition temperature.³² In light of the missing supporting evidence for T_{N3} from the $C_p(T)$ measurement, one may suspect that the existence of T_{N3} from susceptibility data may not be intrinsic. On the other hand, the inability to detect similar kind of first-order phase transition has also been argued in the literature.³² Some other technique like the adiabatic method or a better pulse-sequence design³³ may be needed for measuring small latent heat or entropy change transitions. Although our heat capacity measurements do not support the existence of the T_{N3} phase transition, we must stress that the T_{N3} anomaly has been consistently observed in the magnetization measurements for different batches of powder samples as well as single crystals, i.e., the possibility of contribution from external magnetic impurity phase due to different preparation conditions or contamination can be ruled out. More sensitive heat capacity measurement are being planned to clarify this issue. Overall we conclude that the intrinsic origin

of this transition is an open question.

The entropy change S_M calculated from the magnetic heat-capacity is about 5.63 J/mol K Cu, which is in good agreement with the expected $R \ln(2S + 1)$ (5.76 J/mol K) for $S = \frac{1}{2}$ systems. The S_m value at transition T_{N1} is found to be 2.88 J/mol K Cu, which is 50% of the total entropy and the rest of the entropy is released in the paramagnetic region well above T_{N1} , suggesting the presence of frustrated correlations. The observation of significant entropy well above ordering temperature is generally observed in frustrated spin systems.³⁴ Additionally, nearly all the entropy change has taken place by the time one approaches (with decreasing temperature) the T_{N3} transition. This is the reason I presume that T_{N3} is a weak transition such as a slight canting from the AF ordered state to produce weak FM moment. This might explain the difficulty in observing the transition in heat capacity.

D. Electronic structure calculations

In order to study the electronic structure of $\text{PbCu}_3\text{TeO}_7$, we have carried out first principles density functional theory (DFT) calculations within the local-density approximation (LDA) by employing the Stuttgart TBLMTO-47 code based on the linear muffin-tin orbital (LMTO) method in the atomic sphere approximation (ASA).³⁵ The basis set for the self-consistent electronic structure calculations for $\text{PbCu}_3\text{TeO}_7$ in TB-LMTO ASA includes Pb (s, p), Cu (s, p, d), Te (s, p) and O (s, p) and the rest are downfolded. A (4, 8, 4) k -mesh has been used for self-consistency. All the k -space integrations were performed using the tetrahedron method. In order to ascertain the accuracy of our ASA calculations we also performed the electronic structure calculation using projected augmented wave (PAW)³⁶ method encoded in the Vienna *ab-initio* simulation package (VASP).³⁷ The density of states calculated by these two different approaches is found to agree well with each other. In order to extract various hopping integrals between the Cu atoms, we have employed the N^{th} order muffin tin orbital (NMTO) downfolding method.^{38–40}

The non-spin-polarized band structure for $\text{PbCu}_3\text{TeO}_7$ is displayed in Fig. 6. The bands are plotted along the various high symmetry points of the Brillouin zone corresponding to the orthorhombic lattice. All the energies are measured with respect to the Fermi level of the compound. The characteristic feature of the non-spin-polarized band structure displayed in Fig. 6 is an isolated set of twelve bands crossing the Fermi level and these bands are predominantly derived from the antibonding linear combination of Cu- $d_{x^2-y^2}$ and O-p states. These twelve bands are well separated from the low-lying O-p and other Cu -d valence bands. This isolated Cu- $d_{x^2-y^2}$ twelve

band complex is responsible for the low-energy physics of this compound. Fig. 7 shows the non-spin-polarized density of states (DOS) of $\text{PbCu}_3\text{TeO}_7$. As expected, there is strong hybridization between the O-p and Cu-d states. The occupied Pb-6s states lie below the Fermi level and empty Pb-p and Te-s states are above the Fermi level.

We have employed the NMTO downfolding method to map our LDA results to a low-energy orthogonal tightbinding Hamiltonian by integrating out the high energy degrees of freedom from the all-orbital LDA calculation. The Fourier transformation of the downfolded Hamiltonian $H = \sum_{ij} t_{ij} (c_i^\dagger c_j + h.c.)$ gives the various hopping integrals t_{ij} between the Cu atoms. These hopping integrals will determine the dominant exchange paths for the system. For the present compound we have kept only the Cu- $d_{x^2-y^2}$ orbital for each Cu atom in the unit cell in the basis and integrated out all the rest to derive the low-energy model Hamiltonian. We show the downfolded bands in Fig. 6 in comparison to the full LDA band structure and the agreement between the two is found to be excellent. The hopping integrals (> 10 meV) obtained from the NMTO downfolding method are listed in Table IV and V and the exchange paths are indicated in Fig. 1(f) and 1(g).

The strongest hopping in the Kagome plane is t_3 between the corner-sharing Cu1 and Cu2 ions. This hopping is primarily mediated by O2 situated in the basal plane of the Cu1 octahedron forming a strong $pd\sigma$ antibond with the Cu1 $d_{x^2-y^2}$ orbital. The nn hopping t_1 between the edge sharing Cu1 octahedron (see Fig. 1(c)) and Cu2 tetrahedron (see Fig. 1(d)), is found to be much smaller than t_3 . In order to obtain further insights, we have plotted the Wannier function of Cu2 $d_{x^2-y^2}$ orbital corresponding to the t_3 and t_1 hoppings (see Fig. 8). The plot reveals that the Cu2 $d_{x^2-y^2}$ orbital forms strong $pd\sigma$ antibonds with the neighboring oxygens. We can see that the weight of Wannier function at Cu1 site which is at a distance 3.264 \AA is large compared to the weight at Cu1 site which is at a distance 2.90 \AA indicating t_3 hopping will be stronger in comparison to t_1 . The bond angle of Cu1-O2-Cu2 corresponding to the t_3 hopping is 118.06° , while the bond angle of Cu1-O1-Cu2 is 93° for the t_1 hopping path. The strength of antiferromagnetic interactions are strongly dependent on the angle between the bonds. When the angle is close to 90° , the AF super-exchange process is suppressed due to the orthogonality of Cu 3d and O 2p orbitals. So the exchange coupling along the path t_1 is expected to be ferromagnetic. For t_4 hopping, two Cu1 octahedra are corner-shared with each other and the bond-angle of Cu1-O3-Cu1 is 107° while for the t_2 hopping path, the two Cu1 octahedra share an edge with each other and the bond angle of Cu1-O2-Cu1 is 105° . As argued earlier, the t_4 hopping dominates over the t_2 hopping path due to the corner sharing topology of the Cu1 octahedra. The second strongest hopping is t_7 between the Cu2 atoms. This Cu2-Cu2 hopping primarily proceeds via the oxygens. As a result, the strength

of the Cu-O4-O4-Cu spin exchange is primarily governed by the O-O distance and in this case O-O distance is 2.57 Å (smaller than the van der Waals distance). Moreover, the bond-angle of Cu-O4-O4 is about 167° , which makes this hopping stronger than some of the nn hoppings (t_2 , t_3 , and t_4).

The hopping paths perpendicular to the Kagome plane are listed in Table V. Since the distances between the Cu ions in two different Kagome plane is small, it is expected that there is substantial amount of hoppings between the Kagome planes. The strongest interaction between the Kagome plane is t_2^i . This interaction is mediated via Te following the path Cu-O-Te-O-Cu.

Our electronic structure calculations reveal that intra-kagome and inter-kagome exchange interactions are long ranged. In general, an ideal 2D Kagome system with only uniform nn couplings does not order even at zero- T . However, spin wave theory¹⁶ predicts that the presence of 2^{nd} nn (J_{nnn}) and 3^{rd} nn ($J_{diagonal}$) couplings in the Kagome plane can drive the system to an ordered ground state. When $J_{diagonal} > J_{nnn}$, $\sqrt{3} \times \sqrt{3}$ Néel ordered state is favored, while the $q = 0$ Néel state occurs in the case of $J_{nnn} > J_{diagonal}$. A rich theoretical magnetic phase diagram has also been built based on the type (antiferro and ferromagnetic) and the relative strength ($J_{nnn}/J_{diagonal}$) of interactions in the 2D Kagome system.^{9,17} Since the Kagome plane of $\text{PbCu}_3\text{TeO}_7$ appear to have additional couplings (2^{nd} and 3^{rd} nn), they might support ordered magnetic states as mentioned above. In addition, there are also substantial inter-planar couplings found in this system. These additional intra-Kagome and inter-Kagome couplings might be the reason to have different AF transitions in this system. A detailed neutron diffraction measurements and analysis will however be needed to clarify the origin and nature of these transitions.

IV. CONCLUSIONS

Based on the structural details, one forms the impression that $\text{PbCu}_3\text{TeO}_7$ might have quasi-2D staircase (buckled) Kagome layers. However, our magnetic measurements on polycrystalline and single crystal samples show the onset of LRO at about 36 K with a change in the spin-order around 25 K. This indicates the existence of significant three-dimensional couplings. The $\chi(T)$ is found to obey the simple Curie-Weiss law above 200 K with a Curie constant as expected for a paramagnetic system. However, below 200 K there is a deviation from the Curie-Weiss behavior though it is well above T_N , which suggests the presence of frustrated spin correlations well above T_N . This behavior is also consistent with $C_p(T)$ which infers the presence of magnetic entropy well above the magnetic transitions. We performed electronic structure calculations to determine the relative values and

importance of various exchange paths. Our results suggest the presence of various intra-Kagome (nnn and diagonal) and inter-Kagome exchange hopping paths, which then must be responsible for the onset of LRO in this system. Detailed neutron diffraction measurements will be helpful to understand more about the nature of spin orderings and magnetic phase diagram of this system.

Acknowledgments

The authors FCC and BKR acknowledge the support from National Science Council of Taiwan under project number NSC-100-2119- M-002-021. JC thanks CSIR India (Grant No. 09/080(0615)/2008-EMR -1) for research fellowship. AVM and RK thank the Department of Science and Technology and CSIR, India for financial support. Work at SNU was supported by National Creative Research Initiative (2010-0018300).

* Electronic address: fcchou@ntu.edu.tw

- ¹ G. Misguich and C. Lhuillier, in *Frustrated Spin Systems*, edited by H. T. Diep (World Scientific, Singapore, 2005).
- ² C. Lacroix, P. Mendels, and F. Mila, *Introduction to Frustrated Magnetism* (Springer, Berlin, 2010).
- ³ L. Balents, Nature (London) **464**, 199 (2010).
- ⁴ S. Sachdev, Phys. Rev. B **45**, 12377 (1992).
- ⁵ J. T. Chalker and J. F. G. Eastmond, Phys. Rev. B **46**, 14201 (1992).
- ⁶ S. Yan, D. A. Huse, and S. R. White, Science **332**, 1173 (2011).
- ⁷ M. P. Shores, E. A. Nytko, B. M. Bartlett, and D. G. Nocera, J. Am. Chem. Soc. **127**, 13462 (2005), J. S. Helton et al., Phys. Rev. Lett. **98**, 107204 (2007).
- ⁸ E. Kermarrec, P. Mendels, F. Bert, R. H. Colman, A. S. Wills, P. Strobel, P. Bonville, A. Hillier, and A. Amato, Phys. Rev. B. **84**, 100401(R) (2011), O. Janson, J. Richter, and H. Rosner, Phys. Rev. Lett. **101**, 106403 (2008).
- ⁹ B. Fåk, E. Kermarrec, L. Messio, B. Bernu, C. Lhuillier, F. Bert, P. Mendels, B. Koteswararao, F. Bouquet, J. Ollivier, A. D. Hillier, A. Amato, R. H. Colman, A. S. Wills, Phys. Rev. Lett. **109**, 037208 (2012).
- ¹⁰ P. Mendels et al., Phys. Rev. Lett. **98**, 077204 (2007).
- ¹¹ M. A. Lafontaine, A. L. Bail, and G. Férey, J. Solid State Chem. **85**, 220 (1990).
- ¹² Y. Okamoto, H. Yoshida, and Z. Hiroi, J. Phys. Soc. Jpn. **78**, 033701 (2009).
- ¹³ R. H. Colman, F. Bert, D. Boldrin, A. D. Hillier, P. Manuel, P. Mendels, and A. S. Wills, Phys. Rev. B **83**, 180416(R) (2011).

- ¹⁴ K. Morita, Midori Yano, Toshio Ono, Hidekazu Tanaka, Kotaro Fujii, Hidehiro Uekusa, Yasuo Narumi, and Koichi Kindo, J. Phys. Soc. Jpn. **77**, 043707 (2008).
- ¹⁵ K. Matan, T. Ono, Y. Fukumoto, T. J. Sato, J. Yamaura, M. Yano, K. Morita, and H. Tanaka, Nature Phys. **6**, 865 (2010).
- ¹⁶ A. B. Harris, C. Kallin, and A. J. Berlinsky, Phys. Rev. B **45**, 2899 (1992).
- ¹⁷ J.-C. Domenge, P. Sindzingre, C. Lhuillier, L. Pierre, Phys. Rev. B **72**, 024433 (2005).
- ¹⁸ B. Wedel, H. Mueller-Buschbaum, Zeitschrift für Naturforschung. B **51**, 1587, (1996).
- ¹⁹ N. Rogado, M. K. Haas, G. Lawes, D. A. Huse, A. P. Ramirez, and R. J. Cava, J. Phys. Condens. Matter **15**, 907 (2003).
- ²⁰ N. Rogado, G. Lawes, D. A. Huse, A. P. Ramirez, and R. J. Cava, Solid State Commun. **124**, 229 (2002).
- ²¹ G. Lawes et al., Phys. Rev. Lett. **93**, 247201 (2004).
- ²² G. Lawes et al., Phys. Rev. Lett. **95**, 087205 (2005).
- ²³ <http://www.ccp14.ac.uk/tutorial/powdcell/>
- ²⁴ Juan Rodríguez-Carvajal, Physica B **192**, 55 (1993).
- ²⁵ P. W. Selwood *Magnetochemistry* (Wiley-Interscience, New York, 1956) 2nd ed., Chapter 2, page 78.
- ²⁶ N. Motoyama, H. Eisaki and S. Uchida Phys. Rev. Lett. **76** 3212, (1996).
- ²⁷ A. Daoud-Aladine, B. Kundys, C. Martin, P. G. Radaelli, P. J. Brown, C. Simon, and L. C. Chapon, Phys. Rev. B **80**, 220402 (2009).
- ²⁸ R. Nirmala, Ya. Mudryk, V. K. Pecharsky, and K. A. Gschneidner, Jr., Phys. Rev. B **76**, 104417 (2007).
D. P. Rojas, J. I. Espeso, J. Rodríguez Fernández, J. C. Gómez Sal, J. Sanchez Marcos, and H. Müller, Phys. Rev. B **80**, 184413 (2009).
- ²⁹ D. P. Rojas, J. I. Espeso, J. Rodríguez Fernández, J. C. Gómez Sal, C. Rusu, D. Andreica, R. Dudric, A. Amato, Phys. Rev. B **84**, 024403 (2011).
- ³⁰ Y. Chen, J. W. Lynn, Q. Huang, F. M. Woodward, T. Yildirim, G. Lawes, A. P. Ramirez, N. Rogado, R. J. Cava, A. Aharony, O. Entin-Wohlman, and A. B. Harris, Phys. Rev. B **74**, 014430 (2006), Y. Yasui, Y. Kobayashi, M. Soda, T. Moyoshi, M. Sato, N. Igawa, and K. Kakurai, J. Phys. Soc. Jpn. **76**, 034706 (2007).
- ³¹ Charles Kittel, Introduction to solid state physics, JohnWiley & Sons, Inc., Singapore.
- ³² J. C. Lashley, M. F. Hundley, A. Migliori, J. L. Sarrao, P. G. Pagliuso, T.W. Darling, M. Jaimea, J. C. Cooley, W. L. Hults, L. Morales, D. J. Thoma, J. L. Smith, J. Boerio-Goates, B. F. Woodfield, G. R. Stewart, R. A. Fisher, N. E. Phillips, Cryogenics **43**, 369 (2003), H. Suzuki, A. Inaba, and C. Meingast, Cryogenics **50**, 693 (2010).
- ³³ R.W. Newsome, Jr. and E.Y. Andrei, Rev. Sci Instrum. **75**, 104 (2004).
- ³⁴ L. K. Alexander, N. Büttgen, R. Nath, A. V. Mahajan, and A. Loidl, Phys. Rev. B **76**, 064429 (2007).
- ³⁵ O. K. Andersen and O. Jepsen, Phys. Rev. Lett. **53**, 2571 (1984).
- ³⁶ P. E. Blochl, Phys. Rev. B **50**, 17953 (1994).
- ³⁷ G. Kresse and J. Furthmuller, Phys. Rev. B **54**, 11169 (1996).

³⁸ O. K. Andersen and T. Saha-Dasgupta, *Phy. Rev. B* **62**, R16219 (2000).

³⁹ O. K. Andersen and T. Saha-Dasgupta and R. W. Tank and C. Arcangeli and O. Jepsen, and G. Krier *Springer Lecture Notes in Physics* (Berlin : Springer) Vol. **535** pp. 3–84(2000).

⁴⁰ O. K. Andersen, T. Saha-Dasgupta, and S. Ezhov, *Bull. Mater. Sci.* **26**, 19 (2003).

Figures and captions:

Fig. 1 (a) The crystal structure of $\text{PbCu}_3\text{TeO}_7$ viewed along the b -direction is shown. (b) Projection of staircase (buckled) Kagome planes in the bc -plane formed by Cu and O atoms with various bond-angles¹⁸. The possible nearest neighbor (nn) exchange couplings between Cu1 and Cu2 atoms in the Kagome layer are denoted by J_1, J_2, J_3 , and J_4 . The environments of the Cu1 octahedron, the Cu2 tetrahedron and their coupling are shown in (c), (d), and (e). LDA calculations suggest various hopping paths for (f) intra-Kagome plane and (g) inter-Kagome planes indicated by t_n , and t_n^i , respectively. (color online)

Fig. 2 (a) Powder x-ray diffraction pattern of $\text{PbCu}_3\text{TeO}_7$ at room temperature. The open circles indicate the experimental data, while the calculated XRD with residual factors of $R_p \approx 0.1$, $R_{wp} \approx 0.12$, and $\chi^2 \approx 4$ is shown as a solid red line. The Bragg peak positions are indicated by short-vertical marks and the bottom green line represents the difference between the experimental and calculated data. (b) The x-ray diffraction pattern when the x-rays are incident at the "top" surface of the crystal in the horizontal plane (the incident and the diffracted beam form the vertical plane). The crystallographic axes as determined from Laue diffraction are also illustrated. (color online)

Fig. 3 (a) Magnetic susceptibilities (χ) of a polycrystalline and a single crystal sample are plotted as a function of T . The inset shows an expanded view of the low-temperature data. (b) $(\chi - \chi_0)^{-1}$ is plotted as a function of T . The data are fitted to the Curie-Weiss law in the T -range 200 K - 370 K. (color online)

Fig. 4 Magnetic susceptibility of $\text{PbCu}_3\text{TeO}_7$ in the orientation of $H \parallel a$ for different magnetic fields (a) 1 kOe, (b) 5 kOe, (c) 10 kOe and (d) 15 kOe is plotted. The black solid line indicates zero-field-cooled (ZFC) warming data, while the red and blue solid lines are the data related to field-cooled (FC) cooling and FC warming, respectively. The red and black arrow marks indicate the position of magnetic anomaly in the cooling and warming data, respectively. (color online)

Fig. 5 The C_p data (open circles) are plotted as a function of T . The red solid line is a fit to the equation (see text) in the T -range from 150 K to 280 K and the red dashed line is the extrapolation of the fit. Inset shows magnetic heat capacity (left y -axis) and entropy (right y -axis) versus T . (color online)

Fig. 6 Downfolded band structure (shown in red line) compared to the full orbital band structure (shown in black line) for $\text{PbCu}_3\text{TeO}_7$. (color online)

Fig. 7 Partial density of states obtained from LMTO-ASA. (color online)

Fig. 8 Wannier function of $\text{Cu-d}_{x^2-y^2}$ placed at Cu2 site. (color online)

Tables and captions:

TABLE I: Atomic coordinates, occupancy factors for $\text{PbCu}_3\text{TeO}_7$

Atom	Wyckoff site	x	y	z	occupancy
Pb	4c	0.10691	0.25	0.54683	1
Te	4c	0.38594	0.25	0.30011	1
Cu1	8d	0.38687	0.01543	0.62710	1
Cu2	4c	0.24769	0.25	0.89997	1
O1	4c	0.21017	0.25	0.15840	1
O2	4c	0.30574	0.25	0.68569	1
O3	4c	0.51777	0.25	0.4605	1
O4	8d	0.18466	-0.05591	0.99033	1
O5	8d	0.4347	-0.06281	0.64738	1

TABLE II: The parameters obtained from the Curie-Weiss fit in the temperature range from 200 K to 370 K

	T -range (K)	C ($\text{cm}^3 \text{ K/mol Cu}$)	θ_{CW} (K)	μ_{eff} (μ_B)
$H \parallel a$	200 - 370	0.52 ± 0.05	$-(145 \pm 5)$	2.04
$H \parallel b$	200 - 370	0.49 ± 0.05	$-(155 \pm 5)$	1.98
$H \parallel c$	200 - 370	0.46 ± 0.05	$-(140 \pm 5)$	1.92

TABLE III: The variation of magnetic peak positions of T_{N3} in the cooling and warming $M(T)$ data in different magnetic fields

H (kOe)	T_{N3} (K) (FC cooling)	T_{N3} (K) (ZFC warming)	Difference ΔT (K)
1	15.8 ± 0.1	16.5 ± 0.1	0.7 K
5	16.3 ± 0.1	16.8 ± 0.1	0.5 K
10	17.2 ± 0.1	17.5 ± 0.1	0.3 K
15	17.5 ± 0.1	17.7 ± 0.1	0.2 K

TABLE IV: Hopping (in meV) between various Cu atoms within the Kagome plane, obtained from NMTO downfolding method.

Coupling between	Hopping path	Distance (\AA)	Hopping (meV)	Bond-angle and bond-lengths
Cu1 - Cu2 (nn)	t_1	2.90	46.23	Cu1-O4-Cu2 $\sim 92.9^\circ$, Cu1-O1-Cu2 $\sim 83.1^\circ$
Cu1 - Cu1 (nn)	t_2	3.065	42.17	Cu1-O2-Cu1 $\sim 105^\circ$
Cu1 - Cu2 (nn)	t_3	3.264	149.67	Cu1-O2-Cu2 $\sim 118.1^\circ$
Cu1 - Cu1 (nn)	t_4	3.29	91.16	Cu1-O3-Cu1 $\sim 106.7^\circ$, Cu1-O1-Cu1 $\sim 91^\circ$
Cu2 - Cu2 (nnn)	t_5	5.43	57	O1-O4 $\sim 2.8 \text{ \AA}$, Cu2-O1-O4 $\sim 152^\circ$, O1-O4-Cu2 $\sim 110^\circ$
Cu1 - Cu2 (nnn)	t_6	5.617	19.05	O1-O5 $\sim 2.78 \text{ \AA}$
Cu2 - Cu2 (diagonal)	t_7	6.353	104.76	O4-O4 $\sim 2.57 \text{ \AA}$, Cu2-O4-O4 $\sim 167^\circ$, O4-O4-Cu2 $\sim 167^\circ$
Cu1 - Cu2 (long-range)	t_8	6.7	49	O-O $\sim 2.83 \text{ \AA}$

TABLE V: Hopping parameters (in meV) for inter Kagome plane, obtained from NMTO downfolding method.

Coupling between	Hopping path	Distance (\AA)	Hopping (meV)	Bond-angle and bond-lengths
Cu2 - Cu2	t_1^i	5.92	16.32	
Cu1 - Cu2	t_2^i	6.12	49	Cu1-O3-Te-O4-Cu2, O3-O4 $\sim 2.72 \text{ \AA}$
Cu1 - Cu2	t_3^i	6.27	20.41	
Cu2 - Cu2	t_4^i	6.27	28.53	

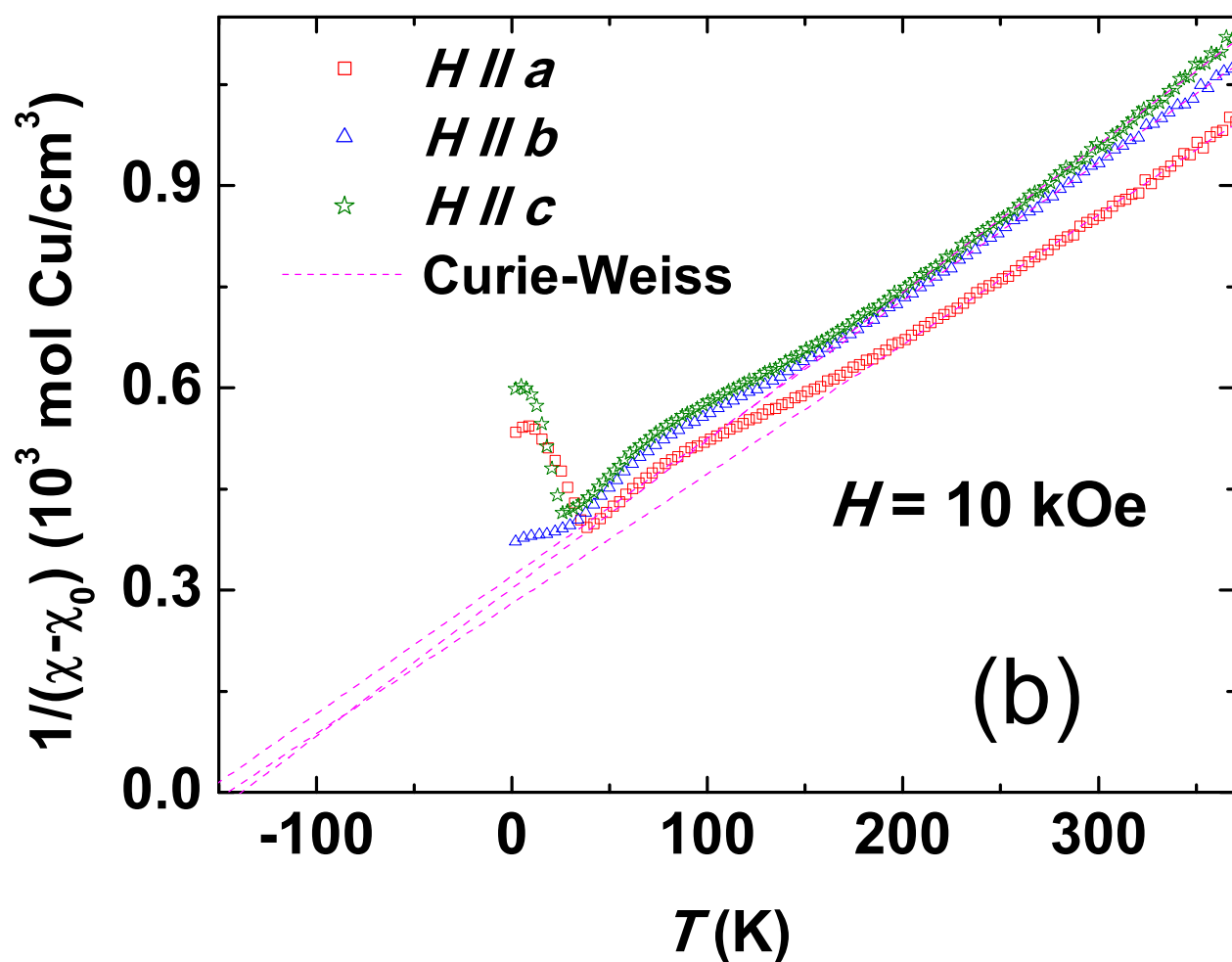
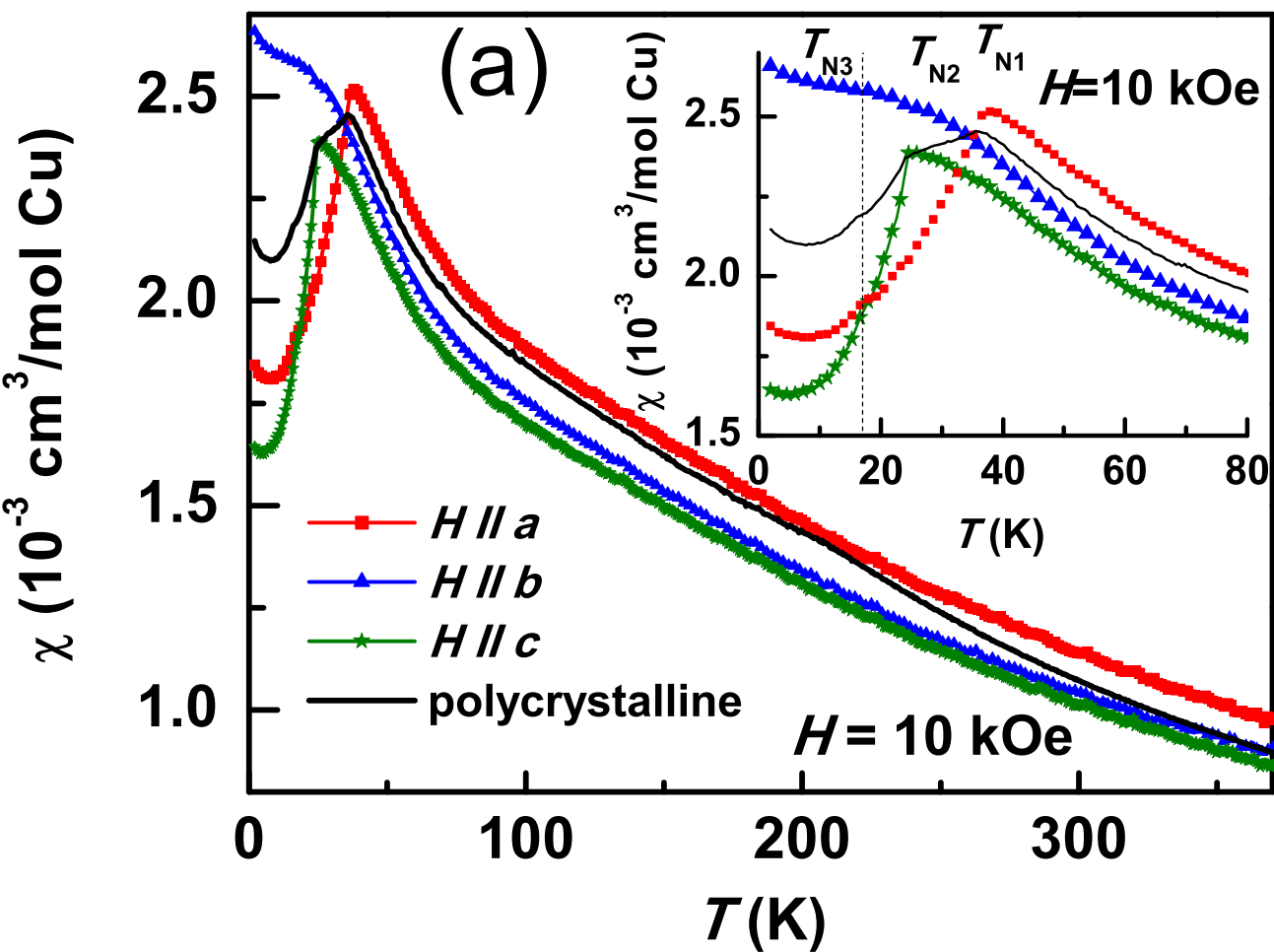


Fig. 3

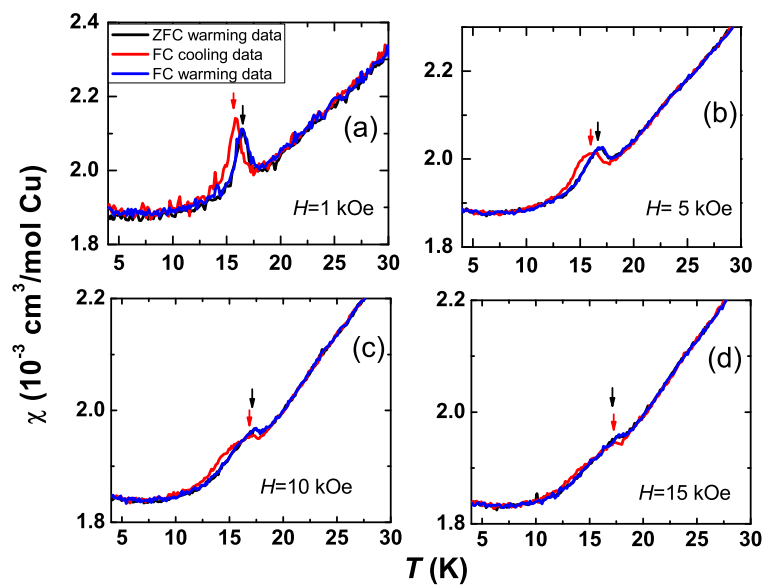


Fig. 4

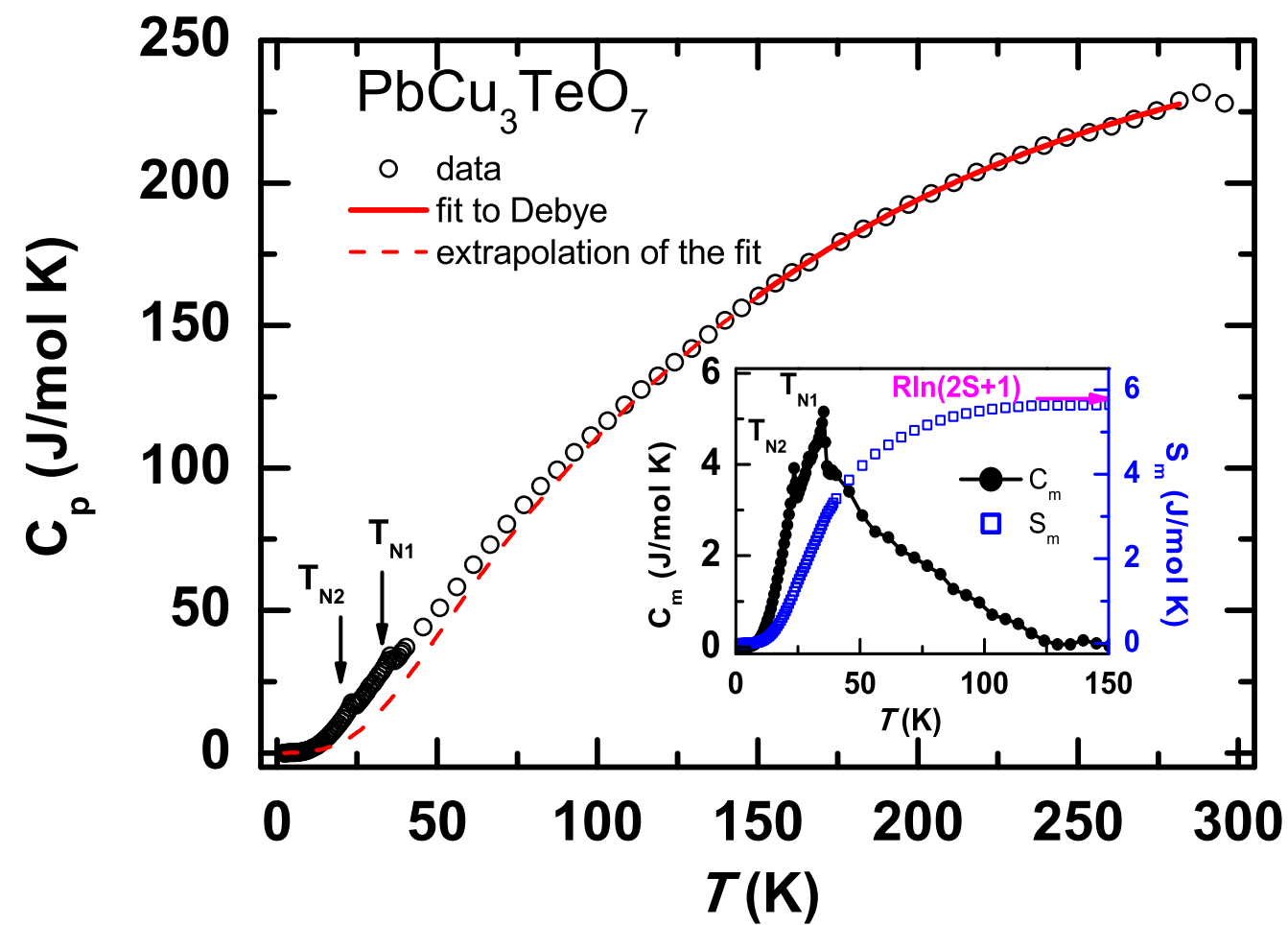


Fig. 5

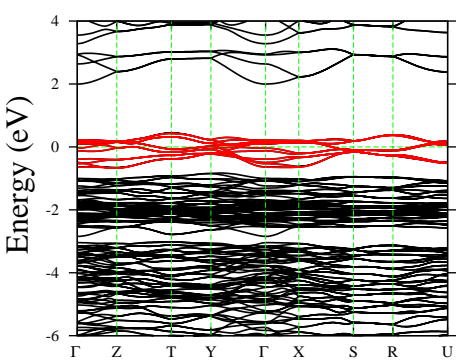


Fig. 6

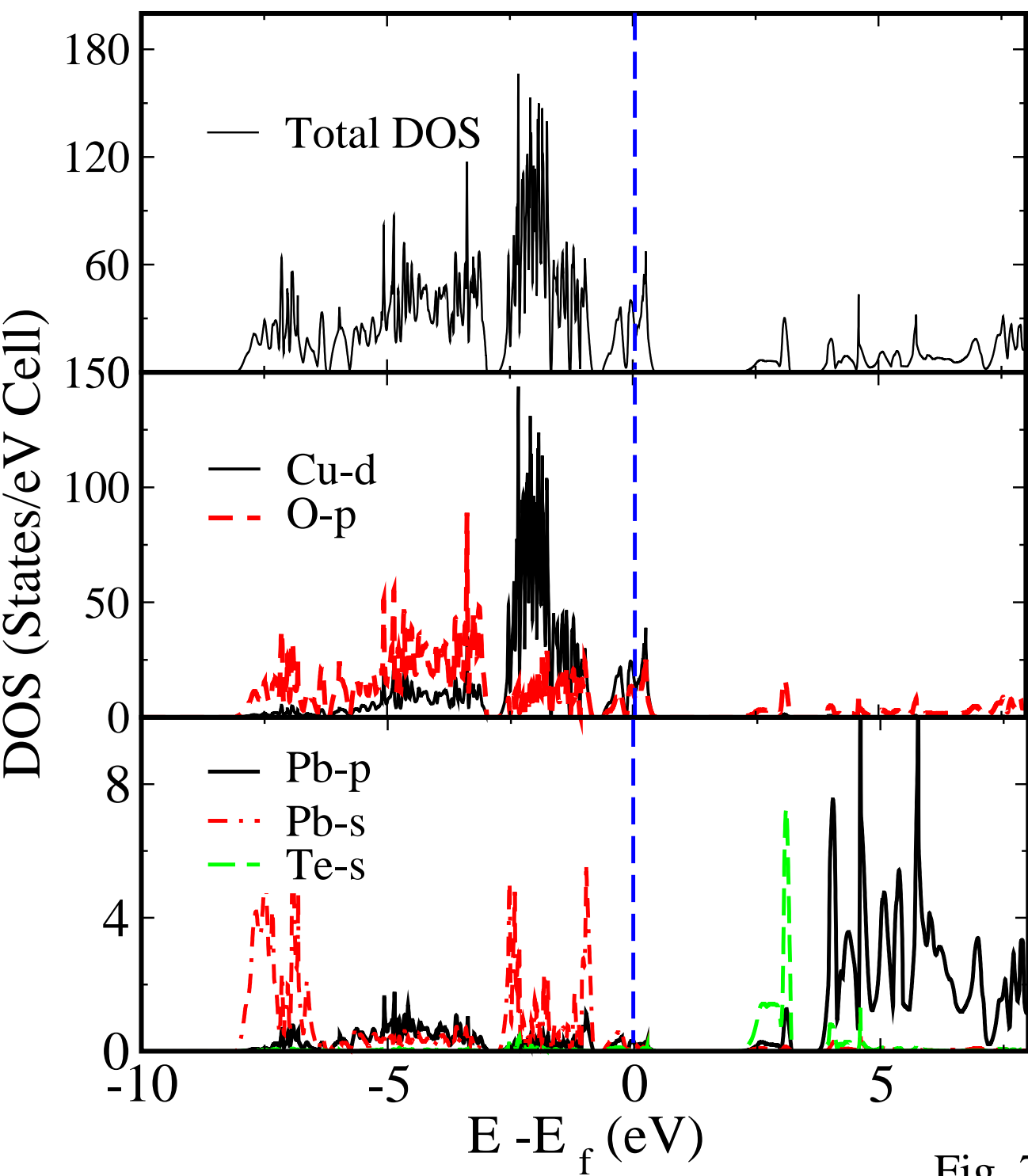


Fig. 7

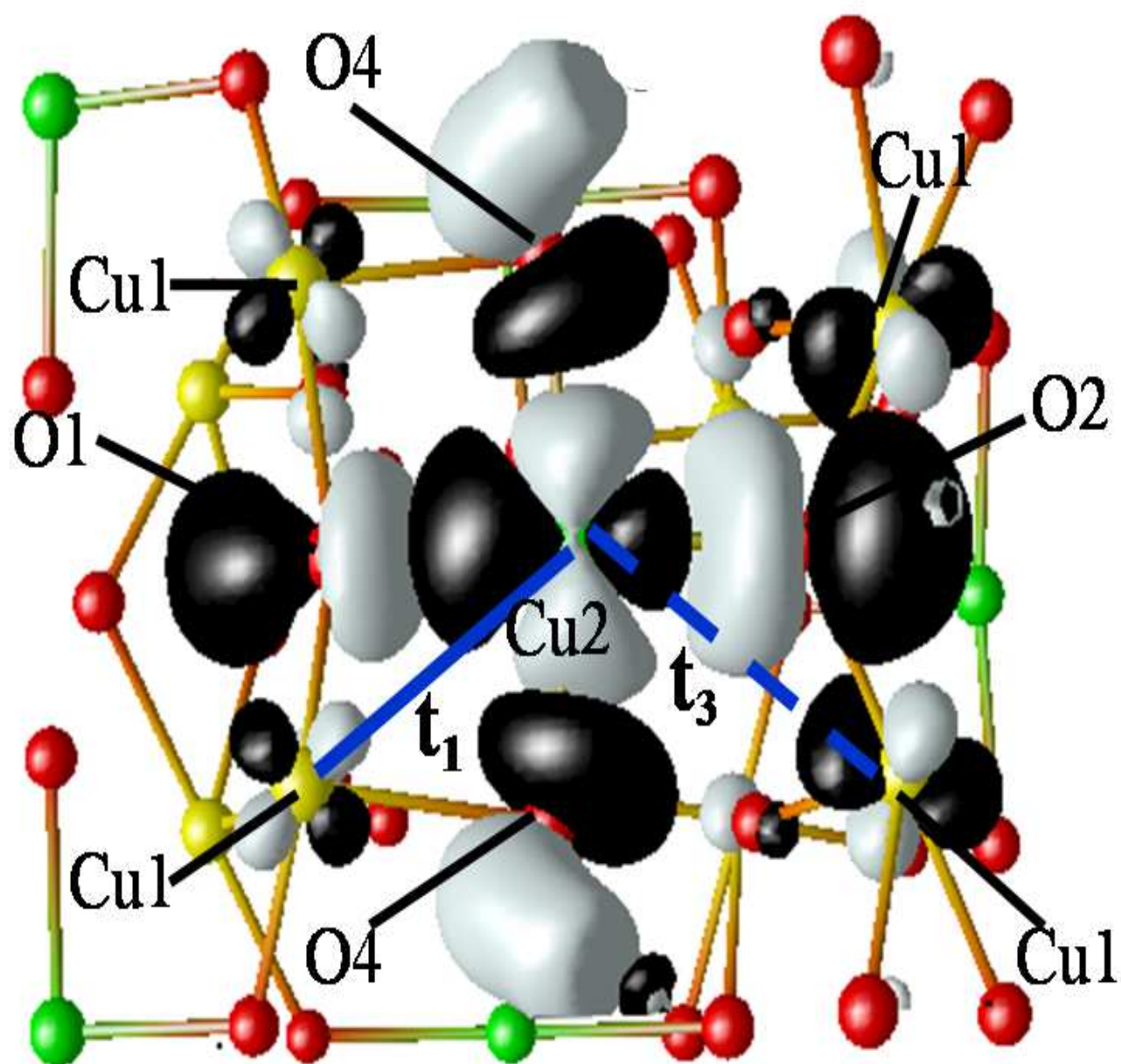


Fig. 8